Lithological and tectonic controls on banded iron formation-associated gold at the Amaruq deposit, Churchill Province, Nunavut, and implications for exploration

Manon Valette[1*], Stéphane De Souza[1], Patrick Mercier-Langevin[2], Olivier Côté-Mantha[3], Marjorie Simard[4], Natasha Wodicka[5], Vicki J. McNicoll[5], and Patrice Barbe[3]

[1]Université du Québec à Montréal, 201 Avenue du Président-Kennedy, Montréal, Quebec H2X 3Y7
[2]Geological Survey of Canada, 490 rue de la Couronne, Québec, Quebec G1K 9A9
[3]Agnico Eagle Mines Ltd., Exploration Division, 765 chemin de la mine Goldex, Val-d'Or, Quebec J9P 7G4
[4]Agnico Eagle Mines Ltd, Technical Services, 10 200 route de Preissac, Rouyn-Noranda, Quebec J0Y 1C0
[5]Geological Survey of Canada, 601 Booth Street, Ottawa, Ontario K1A 0E8
[*]Corresponding author's e-mail: valette.manon8331@gmail.com

ABSTRACT

The Amaruq gold deposit in Nunavut is underlain by the Neoarchean (ca. 2.73–2.63 Ga) supracrustal rocks of the Woodburn Lake group, within the Rae Craton of the Churchill Province. The mineralized zones are hosted in polydeformed, upper greenschist-facies banded iron formation and volcanic and sedimentary rocks of the Rumble assemblage. The assemblage includes rocks of contrasting rheology and geochemistry, such as greywacke, chert, graphitic argillite, komatiite, and komatiitic basalt, which have been deformed and metamorphosed in the Archean and during subsequent Paleoproterozoic orogenesis. In the Amaruq area, several generations of structures are recognized: 1) tight and isoclinal F_1 folds and D_1 shear zones; and 2) upright and isoclinal northeast-plunging F_2 folds and associated D_2 shear zones that host the bulk of gold mineralization. Progressive strain accommodation during D_2 deformation led to the development of north-west-verging overthrust and recumbent F_2 folds. Subsequent deformation consists of open to chevron-style, northeast- and southwest-plunging F_3 folds, and north- and east-striking D_4 and D_5 normal faults and shear zones, respectively. The two principal mineralized areas of the Amaruq deposit, the Whale Tail and IVR, comprise contrasting styles, geometry, and distribution of ore zones in distinct structural domains. The Whale Tail area is primarily characterized by stratabound and locally discordant disseminated to semi-massive pyrrhotite-arsenopyrite-gersdorffite replacement-style orebodies in chert-poor silicate-facies iron formation, and by "silica flooding" zones associated with arsenopyrite-löllingite-pyrrhotite in chert-rich silicate-facies iron formation. The IVR area occurs in an overturned F_2 fold-hinge zone and consists predominantly of shallowly southeast-dipping quartz±carbonate veins that cut the host volcano-sedimentary sequence. Proximal alteration is characterized by variable amounts of Ca-amphibole-feldspar-epidote-muscovite-biotite-carbonate. Petrographic relationships of metamorphic and auriferous sulphide minerals indicate that prograde upper greenschist metamorphism is coeval with D_2 deformation. Native gold was in part exsolved from prograde löllingite during retrograde metamorphism to lower greenschist facies associated with D_3 deformation. The crosscutting relationships between the contrasting ore styles suggest a protracted, multiphase hydrothermal history. The age and relative timing of the gold mineralization represent key issues that are being addressed to help in the development of improved exploration models for banded iron formation-hosted/associated gold deposits in the Churchill Province and other Archean terranes.

INTRODUCTION

The Amaruq deposit, which was discovered in 2013 (Côté-Mantha et al., 2017), is located 120 kilometres northwest of the community of Baker Lake in Nunavut (Fig. 1). It contains a total of 189.1 t of Au (6.08 Moz; reserves and resources) in 46.4 Mt of ore at a grade of 4.07 g/t Au (Agnico Eagle Mines Ltd., December 31, 2018). The deposit is part of a new emerging gold province comprising several mines and gold occurrences associated with Neoarchean supracrustal rocks (Fig. 1), such as (1) the Meadowbank mine hosted in the Woodburn Lake greenstone belt; (2) the Meliadine mine located in the Rankin Inlet greenstone belt; and (3) the Three Bluffs gold occurrences hosted in the Committee Bay belt, which were all deformed and metamorphosed during both the Archean and Proterozoic (Pehrsson et al., 2013a; Sanborn-Barrie et al., 2014; Lawley et al., 2016).

Valette, M., De Souza. S., Mercier-Langevin, P., Côté-Mantha, O., Simard, M., Wodicka, N., McNicoll, V.J., and Barbe, P., 2020. Lithological and tectonic controls on banded iron formation-associated gold at the Amaruq deposit, Churchill Province, Nunavut, and implications for exploration; *in* Targeted Geoscience Initiative 5: Contributions to the Understanding of Canadian Gold Systems, (ed.) P. Mercier-Langevin, C.J.M. Lawley, and S. Castonguay; Geological Survey of Canada, Open File 8712, p. 251–266. https://doi.org/10.4095/326042

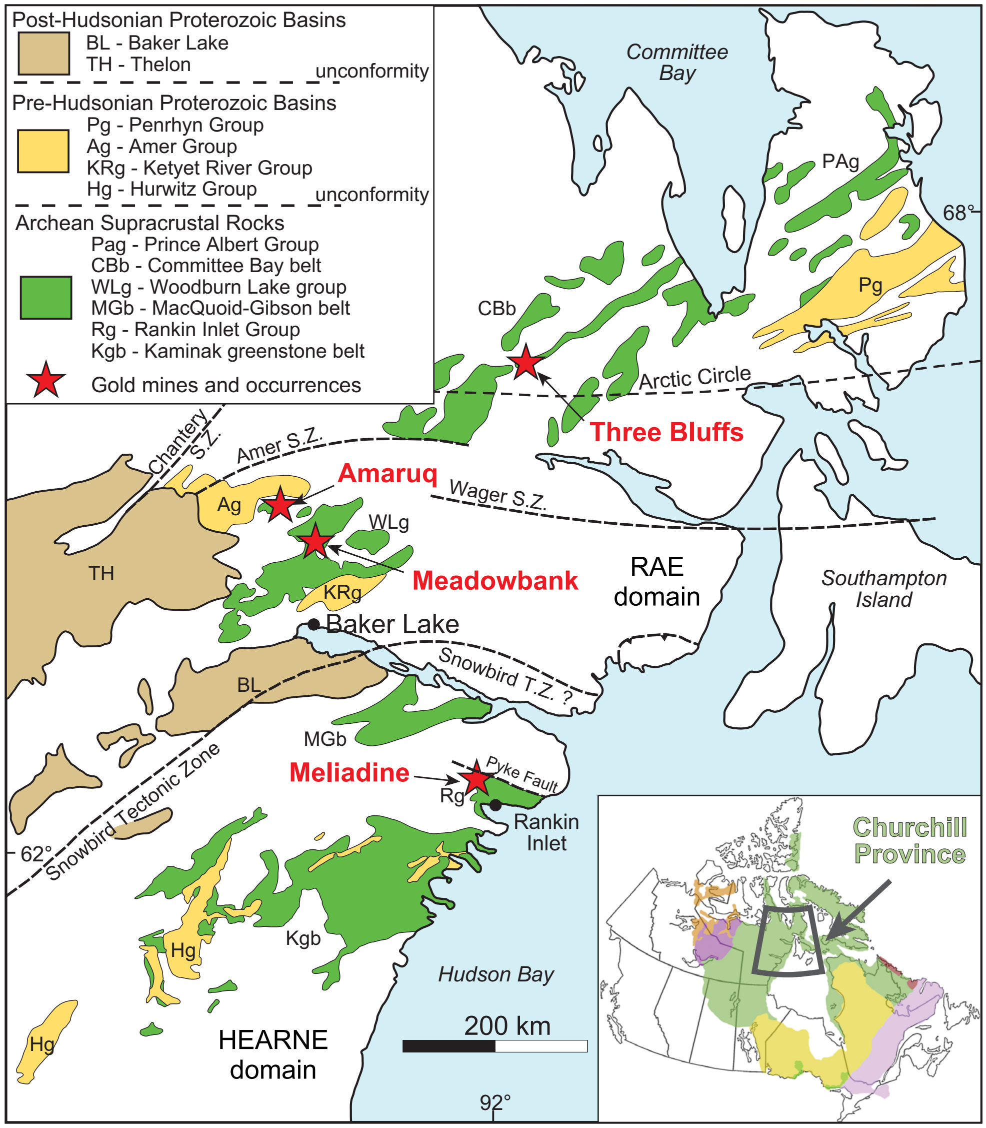

Figure 1. Simplified geological map of the Rae and Hearne cratons of the western Churchill Province showing the location of the Amaruq, Meadowbank and Meliadine mines and Three Bluffs gold occurrence in Nunavut. The white colour represents the undifferentiated Meso- to Neoarchean basement cut by widespread Neoarchean and Paleoproterozoic intrusive suites. The inset shows the distribution of the Churchill Province (*modified from* Valette et al., 2018). Abbreviation: S.Z. = shear zone.

The Amaruq deposit and other gold deposits and occurrences in the region are structurally and lithologically controlled. They are closely associated with crustal-scale faults, shear zones, and/or polydeformed banded iron formation (BIF) units (e.g. Sherlock et al., 2004; Davies et al., 2010; Sanborn-Barrie et al., 2014; Janvier et al., 2015; Lawley et al., 2015, 2016). Even though the bulk of the known gold occurrences in the region are hosted in Archean supracrustal rocks, Trans-Hudsonian orogenesis has controlled most of the structural style and part of the ore-forming events. Previous studies have presented field data, U-Pb monazite and xenotime ages (ca. 1.9–1.8 Ga), and Re-Os arsenopyrite ages from the Meadowbank, Meliadine, and Three Bluffs areas that confirm a Paleoproterozoic Trans-Hudsonian gold mineralizing event (Davies et al., 2010; Janvier, 2016; Lawley et al., 2016). However, 2.3 Ga Re-Os arsenopyrite ages are also obtained at Meliadine (Lawley et al., 2015) and preliminary data at Amaruq indicate that arsenopyrite is systematically older than 2.3 Ga, commonly yielding Archean ages (Mercier-Langevin et al., 2018). These data suggest a complex hydrothermal history, with indications that the mineralized zones are commonly deformed (e.g. boudinage, folding, transposition, and recrystallization) and that gold distribution was probably modified at various scales during deformation and metamorphism (Kerswill et al., 1998; Janvier, 2016; Lawley et al., 2016; Valette et al., 2018). This complexity in age, relative timing, and ore-controlling structures raises questions about the genesis of these deposits.

The working hypotheses are that some significant ore-forming event(s) possibly predate the Trans-Hudsonian Orogeny, and that hydrothermal activity was very long-lived, or, alternatively, the ore-forming event(s) was the result of an incremental process that involved distinct superimposed Archean to Paleoproterozoic gold events. This report summarizes interim results, which are part of an ongoing Ph.D. project that aims to (1) document the geology of the

Amaruq deposit and refine the stratigraphy of the Woodburn Lake group; (2) better constrain the tectonometamorphic evolution of the area; (3) identify the principal controls on gold mineralization; (4) understand how deformation and hydrothermal activity have affected the host rocks and influenced the style, geometry, and distribution of the ore zones; and (5) better constrain the age and relative timing of major ore-forming events.

REGIONAL GEOLOGY

The Amaruq gold deposit is hosted in the Woodburn Lake group of the Rae Craton of the western Churchill Province (Fig. 1). The Rae Craton is composed of a Meso- to Neoarchean (ca. 2.9–2.63 Ga) granodioritic to tonalitic gneissic basement and several Neoarchean greenstone belts (Fig. 1; Berman, 2010; Pehrsson et al., 2013b). The supracrustal rocks form extensive linear belts that are cut by widespread Neoarchean (ca. 2.63–2.58 Ga) granodioritic intrusive rocks of the Snow Island Suite (Berman et al., 2010; Pehrsson et al., 2013b). Paleoproterozoic (ca. 2.3–1.9 Ga) sedimentary basins of the Amer and Ketyet River groups commonly overlay the Archean rocks (Pehrsson et al., 2013a; Jefferson et al., 2015). The Rae Craton has been variably deformed and metamorphosed during several orogenic events: 1) the MacQuoid Orogeny (ca. 2.56–2.5 Ga) on its southeastern margin (Berman et al., 2000; Pehrsson et al., 2013a); 2) the Arrowsmith Orogeny (ca. 2.56–2.28 Ga) on the western edge (Berman, 2010; Pehrsson et al., 2013a); 3) the Taltson-Thelon Orogeny (ca. 1.98–1.91 Ga) on its western margin (McNicoll et al., 2000); and 4) the polyphased Trans-Hudson Orogeny (ca. 1.91–1.81 Ga) on the southeastern edge of the craton (Berman et al., 2005; Pehrsson et al., 2013b). The polyphased Trans-Hudsonian Orogeny coincides with the accretion of the Hearne Craton (ca. 1.9 Ga) and Meta Incognita – Sugluk block (ca. 1.88–1.865 Ga) to the southeastern margin of the Rae Craton, also known as the Snowbird phase, and with the collision of the Sask Craton and Superior Province (ca. 1.84–1.81 Ga) on the south margin of the Hearne Craton (Berman et al., 2013; Pehrsson et al., 2013b).

The Woodburn Lake group (ca. 2.73–2.63 Ga) is divided into six volcano-sedimentary rock assemblages that were affected by two Archean and five Paleoproterozoic deformation events (Pehrsson et al., 2013a). Paleoproterozoic deformation is attributed to the Trans-Hudson Orogeny and is associated with three metamorphic events (Pehrsson et al., 2013a). Following the nomenclature of Pehrsson et al. (2013a), where "A" and "P" represent Archean and Proterozoic deformation events, respectively, D_{A1} and D_{A2} deformation features are only locally and poorly preserved as a schistosity in clasts, and as an axial planar schistosity to small-scale isoclinal folds, respectively (Pehrsson et al., 2013a). D_{A1} fabrics predate 2.71 Ga, the maximum age of the sedimentary rocks comprising the clasts. The second Archean deformation event (D_{A2}) must post-date 2.71 Ga, the age of the rocks of the Woodburn Lake group that are affected by this fabric and may be attributed to the Arrowsmith Orogeny (Berman et al., 2005; Pehrsson et al., 2013a). The D_{P1} shortening event is characterized by tight to isoclinal F_{P1} folds plunging to the south, and by a subhorizontal to shallowly dipping axial planar S_{P1} schistosity. D_{P1} fabrics are affected by tight to isoclinal F_{P2} folds plunging towards the northeast, and by a northeast-trending axial planar S_{P2} schistosity developed during the D_{P2} compressional event. Additionally, northwest-verging thrust faults and shear zones were developed during the D_{P1} and D_{P2} deformation events and caused the repetition of the Archean stratigraphic succession and stacking of the older Archean rocks over younger Paleoproterozoic rocks (Pehrsson et al., 2013a; Calhoun, 2017). Collapse of the Trans-Hudson Orogen then lead to the development of a series of extensional events (Pehrsson et al., 2013a). D_{P3} deformation is characterized by the development of an axial planar S_{P3} crenulation cleavage, associated with shallowly plunging, open to closed, chevron-style F_{P3} folds that are overprinted by north- to northeast-trending, steeply dipping, open to tight F_{P4} folds. The latest structures, associated with the D_{P5} transtensional event comprise a network of east- to northeast-trending extensional shear zones and faults with south-side-down kinematics. These extensional structures are thought to reactivate D_{P2} thrusts, such as the Meadowbank River deformation zone situated between the Amaruq and Meadowbank areas (Pehrsson et al., 2013a; Jefferson et al., 2015; Calhoun, 2017).

The Rae Craton underwent multiple metamorphic events of varying intensity and regional imprint (e.g. Berman et al., 2005; Pehrsson et al., 2013a). In the Committee Bay belt, the first regional metamorphic event, dated at ca. 2.35 Ga, is attributed to the Arrowsmith Orogeny, and could also have affected the rocks of the Woodburn Lake group (Berman et al., 2005). In the Woodburn Lake group, M_{P1} metamorphism is defined by D_{P1} deformation fabrics that are attributed to the Snowbird phase (ca. 1.93–1.91 Ga; Pehrsson et al., 2013a). In both areas, D_{P2} deformation is associated with the main prograde M_{P2} regional metamorphic event (ca. 1.85–1.83 Ga), which is superimposed on the lower metamorphic grade mineral assemblages of the M_{P1} metamorphic event (Pehrsson et al., 2013a). Peak M_{P2} metamorphic conditions increase from lower greenschist facies in the southeast to upper amphibolite facies in the northwest (Berman et al., 2005; Pehrsson et al., 2013a). Retrograde meta-

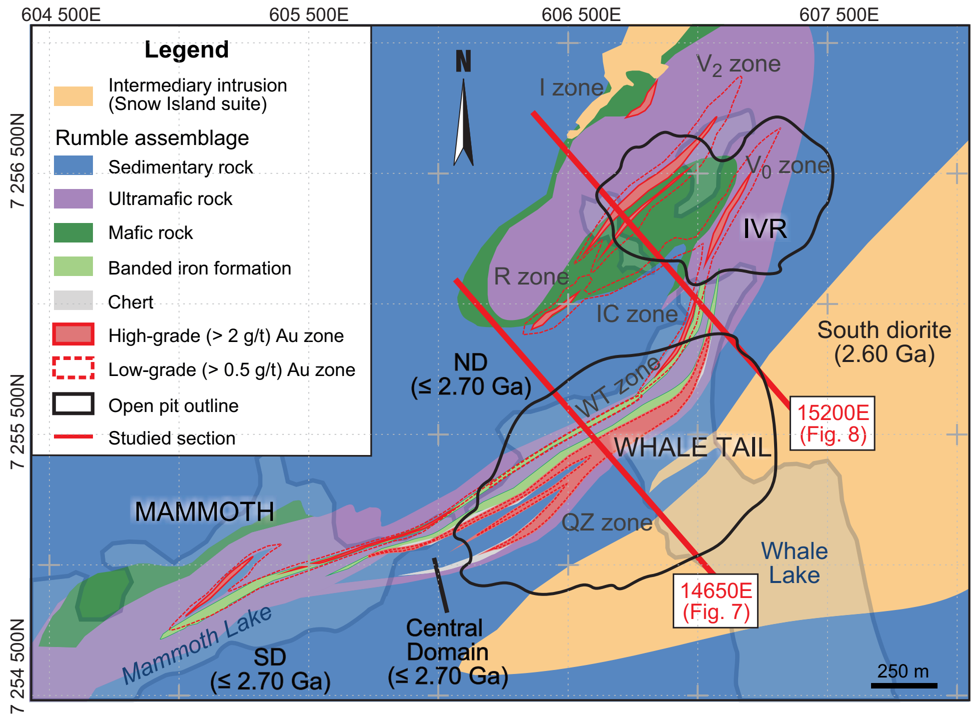

Figure 2. Simplified bedrock geological map of the Amaruq area, showing the location of the Whale Tail and IVR areas and the outlines of the open pits (*modified from* Agnico Eagle Mines Ltd., unpub. data). Abbreviations: ND = north domain, SD = south domain.

morphic conditions are related to M_{P3} metamorphism and are defined by neoblasts aligned in D_{P3} deformation fabrics (ca. 1.82 Ga; Armitage, 1996; Pehrsson et al., 2013a).

LOCAL GEOLOGY

Although the Meadowbank deposit area has been extensively studied over the past two decades (e.g. Pehrsson et al., 2000; Sherlock et al., 2004; Janvier, 2016), only a few regional-scale geological and structural maps are available for the Amaruq area (e.g. Annesley, 1990; Zaleski, 2005; Jefferson et al., 2015; Calhoun, 2017). The Amaruq deposit is hosted in the Rumble assemblage of the Neoarchean (ca. 2735–2630 Ma) Woodburn Lake group, which consists of ultramafic to intermediate igneous rocks, and siliciclastic to chemical sedimentary rocks, including chert and banded iron formation (BIF; Jefferson et al., 2015). The Turqavik-Meadowbank River composite deformation zone, situated 7 km south of the Amaruq deposit, marks the southern boundary of the Rumble assemblage, whereas the northern part is unconformably overlain by the Paleoproterozoic Amer Group (Jefferson et al., 2015).

Deposit Host Rocks and Domains

On the Amaruq property, the Rumble assemblage is characterized by three altered, deformed, and metamorphosed volcanic and/or sedimentary stratigraphic "packages" that are interlayered with silicate (±oxide) facies BIF (Fig. 2, 3). These packages are cut by intrusive diorite bodies (Fig. 2, 3), and by north- and east-striking lamprophyre and felsic dykes, respectively. Two main gold zones, the Whale Tail and IVR orebodies, are present on the Amaruq property (Fig. 2). They both exhibit contrasting ore and alteration styles related to distinct geochemical and structural traps. The Whale Tail area is associated with a laterally and vertically discontinuous central sedimentary domain (central domain: CD) that includes folded and faulted clastic and chemical units. The CD is structurally bounded by two distinct igneous and sedimentary rock packages defined as the south (SD) and north domains (ND) (Fig. 3). Rock units of the SD mainly outcrop south of the Whale Tail area but are also present east-northeast of the IVR area (Fig. 2) due to structural complexities (*see below*). The SD is mainly composed of tightly folded and structurally imbricated greywacke and transitional to calc-alkaline mafic-ultramafic volcanic rocks. The IVR area occurs 300 m northeast of the Whale Tail area (Fig. 2) and comprises the ND, which consists of tholeiitic mafic-ultramafic volcanic rocks and greywacke (Fig. 2). Faults, shear zones, and folds have imbricated and overturned the stratigraphic sequence of the ND, the inferred youngest units of which occur in the core of a recumbent fold hinge (Valette et al., 2018).

Preliminary sensitive high-resolution ion microprobe (SHRIMP) U-Pb geochronology of detrital zircons from the SD, CD, and ND greywackes indicates that these units are all younger than 2.7 Ga. The ND and SD both contain much older zircons (up to 3.15 Ga), whereas the ore-hosting CD has a generally younger zircon population varying between 2.73 and 2.65 Ga. The youngest zircons in the analyzed samples all show evidence of Pb loss and more work is under-

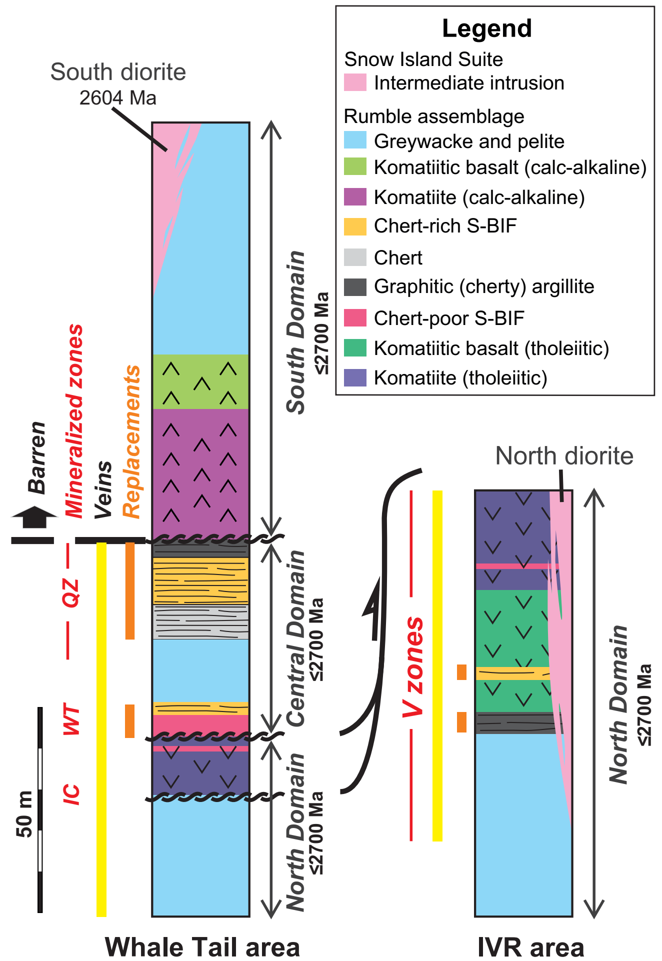

Figure 3. Simplified stratigraphic columns of the Whale Tail and IVR areas showing the location of the principal high-strain and mineralized zones. Abbreviation: S-BIF = silicate-facies banded iron formation.

way to refine the maximum age of the greywacke units of the three domains. A diorite intrusion crosscutting the SD yielded a 2604.9 ± 2.4 Ma age (this study) that falls in the Snow Island Suite age range. The stratigraphic and tectonic relationships between the IVR and Whale Tail orebodies and their host rocks are still under investigation, but structural mapping south of the IVR area suggests that a major shear zone separates the two areas. Thus, until stratigraphic relationships are clarified, two stratigraphic columns are necessary to illustrate the stratigraphy of the Rumble assemblage in the deposit area (Fig. 3).

Host-Rock Petrography

The SD consists of transitional to calc-alkaline mafic to ultramafic volcanic rocks structurally imbricated with greywacke. The volcanic portion comprises green, typically medium-grained, mafic rocks containing hornblende, plagioclase and biotite minerals, and typically dark grey, aphanitic komatiite and komatiitic basalt composed of tremolitic hornblende, phlogopite and albite/oligoclase (Fig. 4a). The mineralogy of the greywacke is homogeneous throughout the study area and mainly consists of millimetre-sized quartz, albite and K-feldspar in a matrix of fine-grained quartz, feldspar, biotite, and minor chlorite. However, the greywacke of the SD is devoid of iron formation and is more homogeneous and less laminated than those of the CD and ND.

Chemical sedimentary units with minor clastic sedimentary layers (i.e. greywacke and siltstone) dominate the CD. It mostly consists, from south to north of (1) a thin graphitic (±cherty) argillite unit (Fig. 4b); (2) mesobanded chert-rich silicate-facies BIF (S-BIF; Fig. 4c) and microbanded chert units; (3) a thicker central unit of greywacke and siltstone; and (4) an upper unit of mesobanded chert-rich S-BIF in contact with (5) chert-poor S-BIF (Fig. 4d). The chert-rich S-BIF is mainly composed of millimetre-thick alternating layers of chert with grunerite, ferrostilpnomelane, ripidolite, and magnetite (Fig. 4c), whereas the chert-poor BIF is a brownish dark green, locally laminated rock composed of hornblende, biotite, ferrostilpnomelane, ripidolite, and almandine garnet (Fig. 4d). In the ND, ultramafic rocks are alternating with chert-poor S-BIF, whereas mafic volcanic rocks and greywacke are intercalated with graphitic (±cherty) argillite and chert-rich S-BIF, respectively (Fig. 3).

The ND consists of tholeiitic mafic to ultramafic volcanic rocks structurally underlain by greywacke. The tholeiitic ultramafic rocks show local spinifex texture (Fig. 4e) and polyhedral jointing. These rocks consist predominantly of bluish gray and aphanitic komatiite and komatiitic basalt composed of tremolite, pycnochlorite, and talc with trace amounts of chromite, magnetite and Ni-Fe-sulphides such as nickeline and gersdorffite. The mafic portion consists of greenish and brownish, medium- to fine-grained volcaniclastic (Fig. 4f) and gabbroic rocks, which are mainly composed of actinolite or Mg-hornblende with ripidolite, clinozoisite, calcite, and minor titanite. A two metre-thick marker horizon of graphitic argillite outlines the contact between the mafic volcanic rocks and the greywacke of the ND (Fig. 3).

Host-Rock Geochemistry

Two geochemically distinct, mafic-ultramafic volcanic rock packages in the SD and ND were identified by whole-rock geochemistry and portable X-ray fluorescence (pXRF) analyses, which helped to reliably map the deposit geology throughout the exploration stages (Côté-Mantha et al., 2017). These two packages cannot be distinguished based on the Jensen (1976) classification diagram and mainly plot in the komatiite, komatiitic basalt, and high-Mg and high-Fe tholeiitic basalt fields (Fig. 5a). These can however easily be distin-

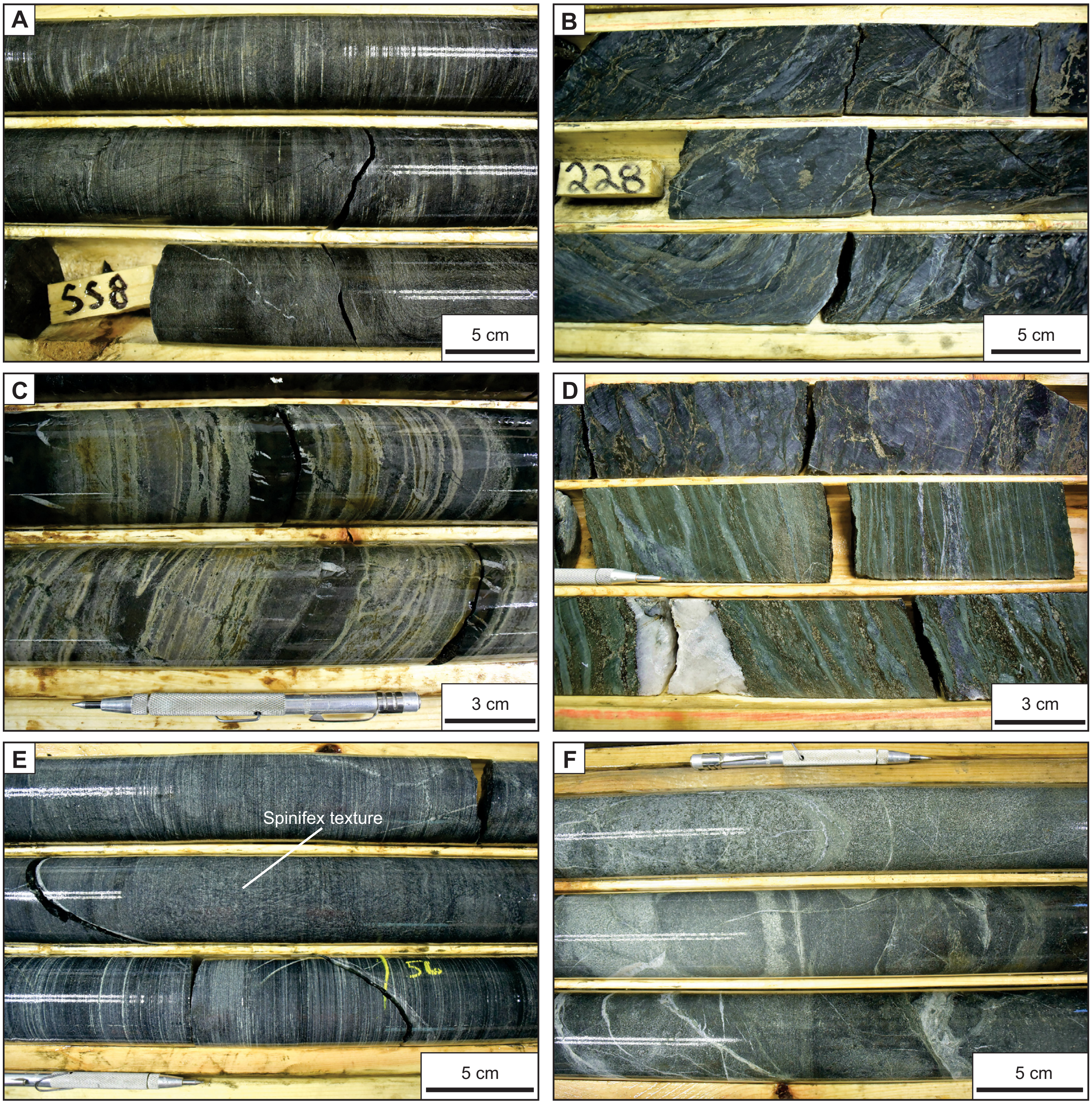

Figure 4. Photographs of the least altered lithologies present at Amaruq. **a)** The komatiite volcanic rock with a calc-alkaline magmatic affinity of the SD zone. **b)** The graphitic (cherty) argillite of the CD zone. **c)** The mesobanded chert-rich silicate-facies banded iron formation (S-BIF) of the CD zone. **d)** The mesobanded chert-poor S-BIF of the CD zone. **e)** The komatiite volcanic rock with a tholeiitic magmatic affinity of the ND zone. **f)** The mafic volcaniclastic rock of the ND zone.

guished on a Zr versus Y magmatic affinity diagram (Fig. 5b) and on a chondrite-normalized rare earth elements (REE) diagram (Fig. 5c). The mafic-ultramafic volcanic rocks of the ND have a typical tholeiitic signature, whereas those of the SD have transitional to calc-alkaline geochemical affinity.

The different sedimentary rocks at Amaruq can also be geochemically distinguished (Fig. 5d). The phyllosilicate-dominated chert-poor S-BIF has a higher Al-ratio and lower Fe-ratio, than the amphibole- and chert-rich S-BIF, which is interpreted to have a greater hydrothermal component (cf. Spry et al., 1998). The higher input of hydrothermal elements to the chert-rich S-BIF is supported by a positive Eu anomaly, which is generally interpreted as being associated with high-temperature and reduced hydrothermal fluids (Fig. 5c; Spry et al., 1998). The chert-poor S-BIF has a flat to slightly light-REE depleted signature, whereas the

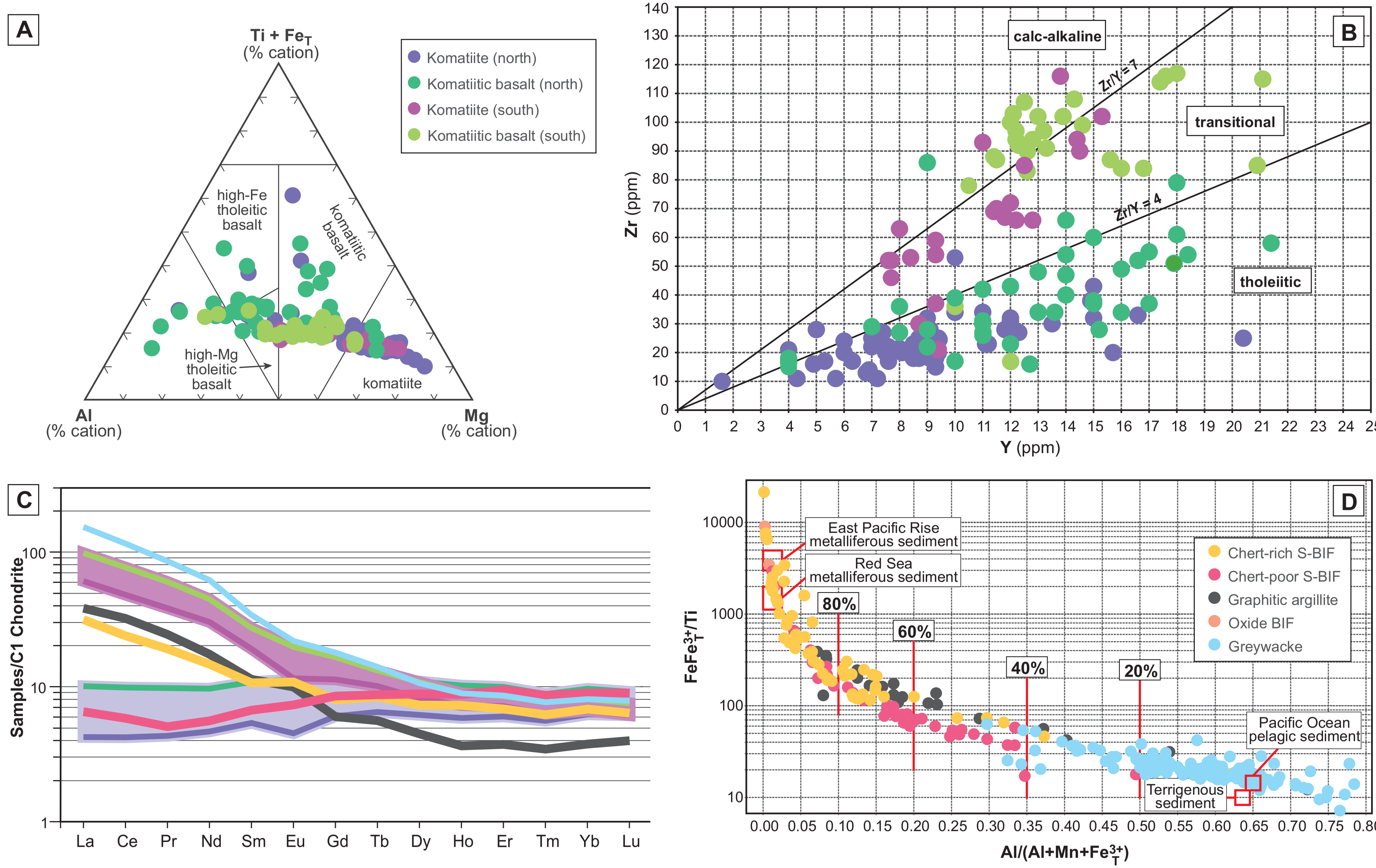

Figure 5. Geochemical diagrams for the classification and characterization of the protoliths of the Amaruq area. **a)** AFM ternary diagram of Jensen (1976), and **b)** Zr versus Y magmatic affinity diagram from MacLean and Barrett (1993) for igneous rocks. The legend is the same for plots (a) and (b). **c)** C1 chondrite normalized rare earth element profile envelops or average of the host rocks of the Amaruq deposit (McDonough and Sun, 1995). The legend is the same plots (c) and (d). For the igneous rocks, polygons represent the transition from komatiite to komatiitic basalts. **d)** Diagram of Fe^{3+}_T/Ti versus Al/(Al+Mn+Fe^{3+}_T) ratios to estimate the hydrothermal contribution to the sedimentary rocks with plots of the average of Pacific Ocean pelagic sediment, terrigenous sediment, as well as the Red Sea and East Pacific Rise metalliferous sediments (Boström, 1973).

chert-rich S-BIF is enriched in light-REE (Fig. 5c). The graphitic argillite has a strongly heavy-REE depleted signature. The SD, CD, and ND greywackes are strongly light-REE enriched and show fractionated REE patterns, as the chert-rich S-BIF and the graphitic argillite (Fig. 5c).

DEFORMATION AND METAMORPHISM

The structural geology of the Amaruq area is complex and, except for the IVR area, exposure is poor, hampering a complete documentation of the polyphase structural styles and geometric relationships among the strongly deformed ore zones. The different generations of fabrics in the Amaruq area are compared and correlated with the regional deformation phases of Pehrsson et al. (2013a) and summarized in Table 1.

The earliest recognized deformation event (D_1) at Amaruq is manifested by isoclinal to tight F_1 folds and the associated axial planar S_1 foliation defined by alignment of phyllosilicate minerals. D_1 fabrics were affected by tight to closed, gently to moderately, east- to northeast-plunging F_2 folds. The D_1 fabrics were variably transposed subparallel to the moderately (50°) southeast-dipping axial planar S_2 schistosity (Fig. 6a,b). Complete transposition of the S_1 foliation results in a composite $S_{1\text{-}2}$ schistosity on the F_2 folds limbs. S_2 schistosity is penetrative in all rock types, except in the chert-rich S-BIF where it is developed as a centimetre-spaced cleavage (Fig. 6a). A moderately to steeply southwest-plunging (45–70°) L_{m2} mineral lineation is defined by alignment of phyllosilicate minerals (e.g. chlorite).

Progressive strain accommodation led to the development of recumbent F_2 folds and south-dipping thrust faults and/or shear zones that are subparallel to the S_2 schistosity. Some faults may have been initiated during D_1 deformation and reactivated during D_2 deformation. One of these mineralized shear zones is well exposed between the Whale Tail and IVR areas and corresponds to the IC zone (Fig. 1, 6c). Compressive shearing fabrics (i.e. C/S fabrics) and quartz vein boudins indicate northwest-directed transport along these shear zones. Shearing and faulting observed in drill core along the overturned limbs of F_1 and/or F_2 folds in the most competent rocks (e.g. S-BIF) are interpreted to represent overthrusts that controlled the localization of the mineralized zones at smaller scale.

The D_2 deformation fabrics are folded by asymmetric, open to closed, chevron-style F_3 folds (Fig. 6d,e,f), which are associated with the development of shallow north- and south-dipping S_3 crenulations that define a conjugate cleavage set. The S_3 crenulations are poorly developed in chert-rich S-BIF but are preferentially developed near or within high-strain zones, as well as in fold-hinge zones affecting the volcanic and sedimentary rocks. The $L_{2\text{-}3}$ intersection lineation is shallowly plunging (0–20°) towards the northeast or southwest, and is subparallel to the F_2 and F_3 folds axes. The L_{m2} and the $L_{1\text{-}2}$ intersection lineation are only locally preserved on the long and south-dipping limbs of the asymmetric F_3 folds. Younger fabrics are characterized by northeast- to northwest-striking, steeply dipping, centimetre-spaced cleavage and normal faults (D_4 deformation), and steeply dipping, east-striking shear zones (D_5 deformation) preferentially developed in the less competent rocks (e.g. ultramafic volcanic rocks of the ND).

Petrographic and microstructural relationships between fabrics and metamorphic minerals, such as garnet porphyroblasts, provide evidence for syn- to late-D_2 peak metamorphism at upper greenschist facies (Fig. 6e). Peak metamorphic conditions overprint part of the ore-associated sulphides, which also show textural evidences of prograde and retrograde transformations, such as triple junctions and inclusion of löllingite in arsenopyrite (Lauzon et al., 2020). A retrograde greenschist-facies metamorphic event (M_3) is marked by andalusite crystals aligned along the S_3 crenulation cleavage in sedimentary rocks and pseudomorphs of M_2 metamorphic minerals (Fig. 6f).

ORE ZONES: STYLES, DISTRIBUTION, AND HYDROTHERMAL ALTERATION

At Amaruq, the high-grade gold zones are preferentially developed along lithological contacts between specific units, within structural traps such as brittle-ductile high strain zones, or F_2 fold hinges (Fig. 7, 8). The bulk of the gold is hosted in the BIF of the CD at Whale Tail (Fig. 3, 7), whereas a significant amount of gold in the IVR area occurs in quartz±calcite veins crosscutting the volcano-sedimentary sequence of the ND (Fig. 8). The mineral assemblage, intensity, and width of the hydrothermal alteration halo vary with the host rocks and style of mineralization. In general, the mineralized zones are characterized by a proximal Ca-enriched metasomatic alteration halo surrounded by a distal K- and/or Na-enriched envelope (Fig. 9a,b,c,d). The proximal alteration halo is characterized by a sulphidation front (pyrrhotite and arsenopyrite) locally associated with silicification of the chemical sedimentary rocks (Fig. 9a). Gold is present as inclusion in idioblastic arsenopyrite (Fig. 9e,f), pyrrhotite or gersdorffite, at sulphide crystal boundaries (Fig. 9e), as fracture-filling in sulphides, and as free grains (Fig. 9g) in quartz-rich rocks (i.e. veins, silicified zones, and chert).

Whale Tail Area

In the Whale Tail area, the chert-poor S-BIF is one of the principal hosts to ore, which consists of stratabound

Table 1. Summary of the main deformation events and fabrics present at Amaruq, and regionally in the Woodburn Lake group. Compiled from Pehrsson et al. (2013b), Jefferson et al. (2015), Janvier (2016), and Valette et al. (2018).

Events	Orientation	Archean rocks of the Amaruq area (this study)			Events	Orientation	Archean rocks of Woodburn Lake (Pehrsson et al., 2013)		
		Planar	Linear	Fold geometry			Planar	Linear	Fold geometry
Note: Archean fabrics are either not present at Amaruq, or more likely completely overprinted by Proterozoic fabrics		-	-	-	D_{A1} (pre-date 2.71 Ga)	-	Internal schistosity and foliation in lithic clasts	-	-
		-	-	-	D_{A2} (post-date 2.71 Ga) but pre-date KRg)	-	Axial planar schistosity	-	Outcrop-scale isoclinal folds
D_1	N-S or E-W compression?	Axial planar and folded penetrative schistosity Thrust faults/shear zones	$L_{0\text{-}1}$ intersection lineation	Cylindrical Symmetric Tight to Isoclinal	D_{P1} (1.93–1.91 Ga)	NNE-SSW compression	Axial planar subhorizontal to shallowly dipping schistosity, slaty cleavage or clast flattening Grain shape fabric in plutonic rocks Subparallel to bedding or compositional layering D_{P1} thrusts that allow intercalated sequence (evident in ultramafic volcanic rocks)	-	At all scales Isoclinal Inclined to recumbent tight to isoclinal N-, NW-, or NE-dipping axial surfaces
D_2	WNW-ESE compression	Mostly subvertical ENE-WSW axial planar and penetrative schistosity or cleavage SE-dipping brittle-ductile reverse faults/shear zones	SW (or SE depending on D_3) moderately to steeply plunging mineral lineation that is locally subparallel to $L_{1\text{-}2}$ intersection lineation	Cylindrical Symetric Upright to recumbent Isoclinal Tight to closed	D_{P2} (1.88–1.865 Ga)	NW-SE compression	The predominant map-scale structures NE-trending axial planar slaty to crenulation cleavage or schistosity, which is locally more intense (development of shear zone) on overturned limbs of F_{P2} folds Thinning and truncation of units and development of reverse fault on these limbs NW-vergent fold thrust belt with basement and cover thrust stacking (S or SE side up to the N or NW)	L_{P2} crenulation lineation or mineral elongation subparallel to F_{P2} fold hinges Strong downdip stretching lineation on S-dipping limbs affected by shear zone	At all scales NE-trending NW-vergent Close to isoclinal
D_3	NNW-SSE compression	Subhorizontal NE-SW axial planar crenulation cleavage (mm to dm)	Subhorizontal $L_{2\text{-}3}$ intersection lineation that is subparallel to F_2 and F_3 fold axes	Non cylindrical Assymetric Open to closed Chevron-style	D_{P3} (1.82 Ga)	NW-SE compression	Axial planar crenulation cleavage Inhomogeneously distributed Moderately to shallowly N- and NE-dipping axial surfaces (40°) Rarely found north of the MRDZ Intensity increases to the south with discrete shallow-dipping shear zones parallel to axial surfaces	Subhorizontal plunging fold axis (20°) L_{P3} crenulation lineation parallel to F fold axes	SE vergence Open to closed Chevron to similar
D_4	NW-SE transtension/ extension	N-S subvertical centimetre-spaced cleavage and faults (E- and W-dipping) ± kink bands	-	-	D_{P4} (1.78–1.735 Ga)	NNW-SSE compression	NNE-trending and steeply dipping (>60°) axial surfaces A local crenulation cleavage Dome & basin (type-1) fold interference with F_{P3} folds	Coarse-spaced L_{P4} crenulation lineation Doubly plunging Plunge direction controlled by the limb dips of older F_{P2} and F_{P1} folds	Map- to outcrop-scale Open to tight Upright moderately to shallowly plunging angular to chevron style
D_5	NW-SE transtension/ extension	E-W shear zones	-	-	D_5 (1.76–1.75 Ga)	NW-SE transtension /extension	ENE-trending brittle-ductile extensional shear zones and faults with S- and N-sides down Reactivate DP_2 structures (e.g. MRDZ)	-	-

Abbreviations: KRg = Ketyet River group, MRDZ = Meadowbank River deformation zone.

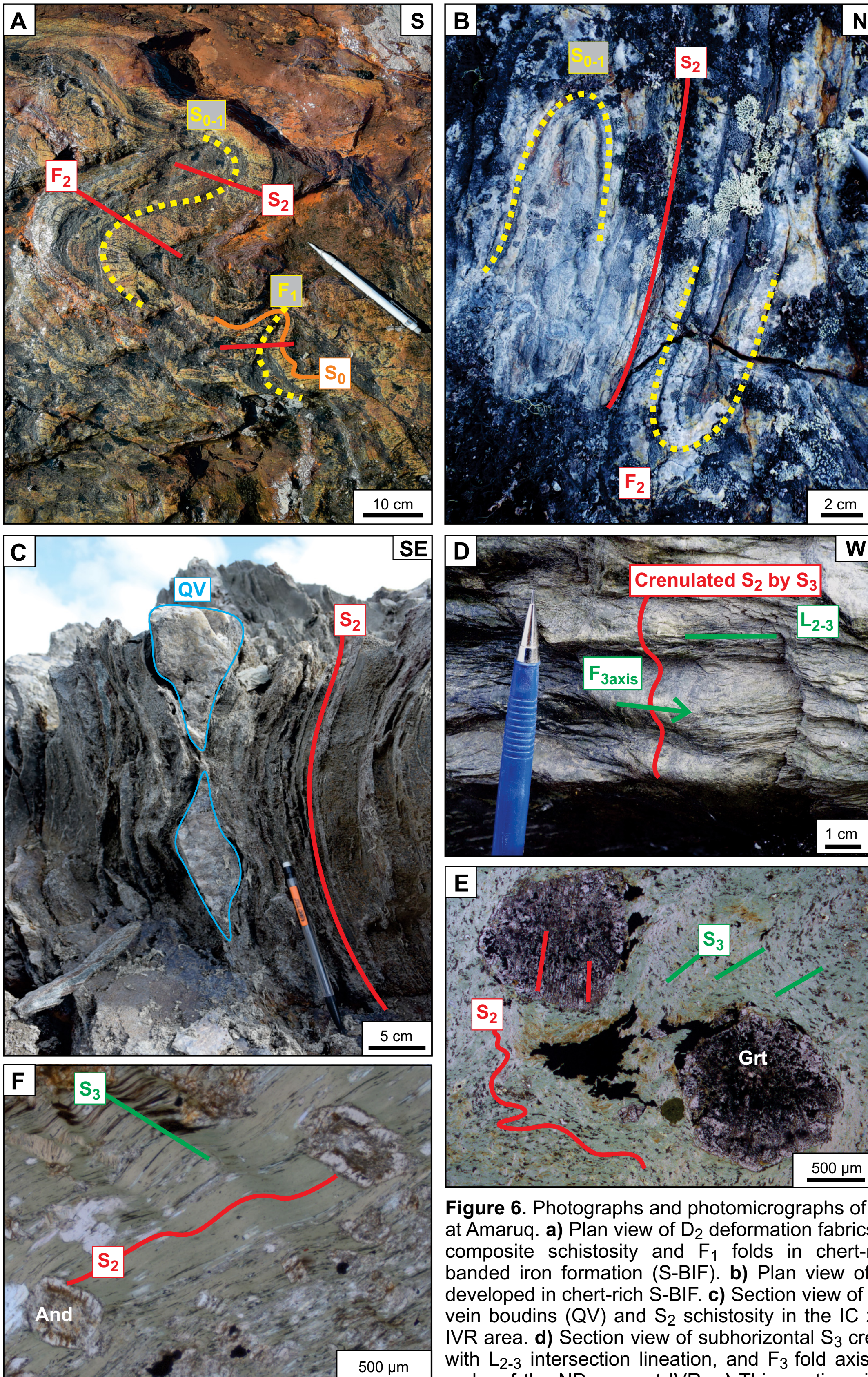

Figure 6. Photographs and photomicrographs of structures present at Amaruq. **a)** Plan view of D_2 deformation fabrics affecting the $S_{0\text{-}1}$ composite schistosity and F_1 folds in chert-rich silicate-facies banded iron formation (S-BIF). **b)** Plan view of isoclinal F_2 folds developed in chert-rich S-BIF. **c)** Section view of asymmetric quartz vein boudins (QV) and S_2 schistosity in the IC zone, south of the IVR area. **d)** Section view of subhorizontal S_3 crenulation cleavage with $L_{2\text{-}3}$ intersection lineation, and F_3 fold axis in mafic volcanic rocks of the ND zone at IVR. **e)** Thin section view of garnet (Grt) porphyroblasts containing the S_2 schistosity, which is crenulated by S_3 crenulation cleavage in chert-poor S-BIF. **f)** Plane-polarized thin section view of andalusite (And) crystals superimposed on S_2 schistosity and aligned along the S_3 crenulation cleavage in greywacke.

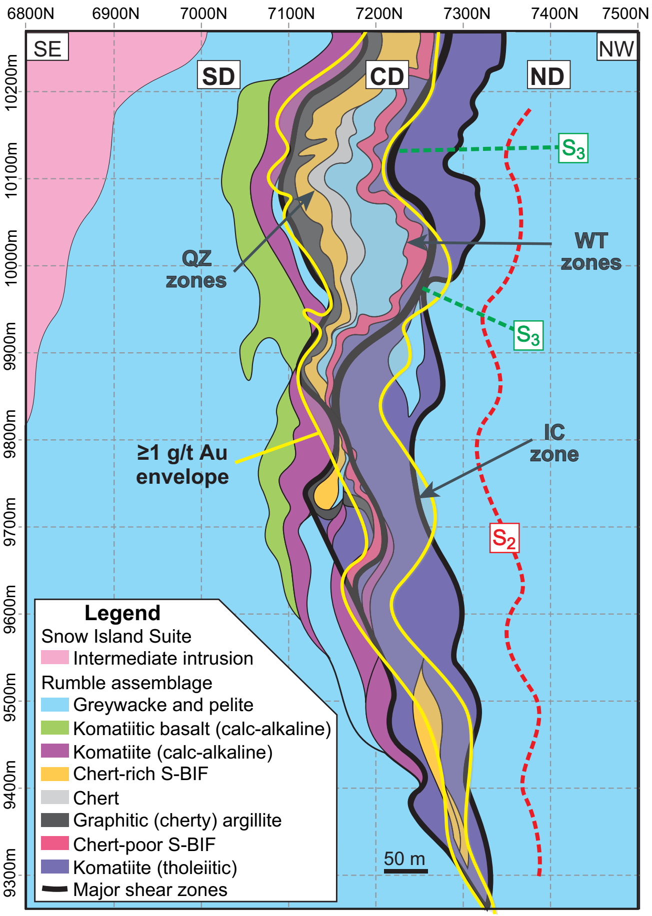

Figure 7. Interpretative cross-section of the Whale Tail (14600 E) area based on drill section. *See* Figure 2 for location of the section. Abbreviation: S-BIF = silicate-facies banded iron formation.

disseminated and replacement-style zones that are locally discordant (WT zones: Fig. 2, 6, 9b). The ore-bearing BIFs occur at the northern contact of the CD or intercalated within the tholeiitic komatiitic rocks of the ND (Fig. 7). It is mainly characterized by finely disseminated pyrrhotite-arsenopyrite±gersdorffite (Fig. 9f). Veins and veinlets are composed of actinolite-quartz±calcite, whereas the replacement zones comprise Ca-amphibole-siderophyllite-clinozoisite-garnet±apatite–titanite. This style of ore typically yields 5 to 7 g/t Au over 6 to 8 m intervals (Côté-Mantha et al., 2017). Ore in the southern part of the CD (QZ zones), consists of sharp to diffuse silicified zones (i.e. "silica flooding") within the chert-rich S-BIF (Fig. 7, 9a), and quartz veins in chert (Fig. 9c) and greywacke. Both styles of ore are mainly associated with coarse idioblastic arsenopyrite±löllingite as the main ore-related minerals. In the chert-rich S-BIF, the hydrothermal assemblage is composed of a distal zone of ripidolite-ferrostilpnomelane-siderophyllite-garnet, and a proximal ferroactinolite-calcite±apatite zone (Fig. 9a). The alteration of chert layers is characterized by a sequence of distal K-feldspar-biotite, outer proximal clinozoisite, and inner proximal actinolite-plagioclase-calcite±ilmenite/titanite zones (Fig. 9c). Mineralized intervals typically yield 4 to 5 g/t Au over 4 to 5 m intervals (Côté-Mantha et al., 2017).

The WT and QZ gold zones form a broad, steeply dipping to subvertical, F_2 and F_3 folded mineralized envelope (≥1 g/t Au; Fig. 7). Ore zones have an average thickness of 2 to 5 m, but they locally reach up to 18 m in thickness, especially in fold hinge zones. The miner-

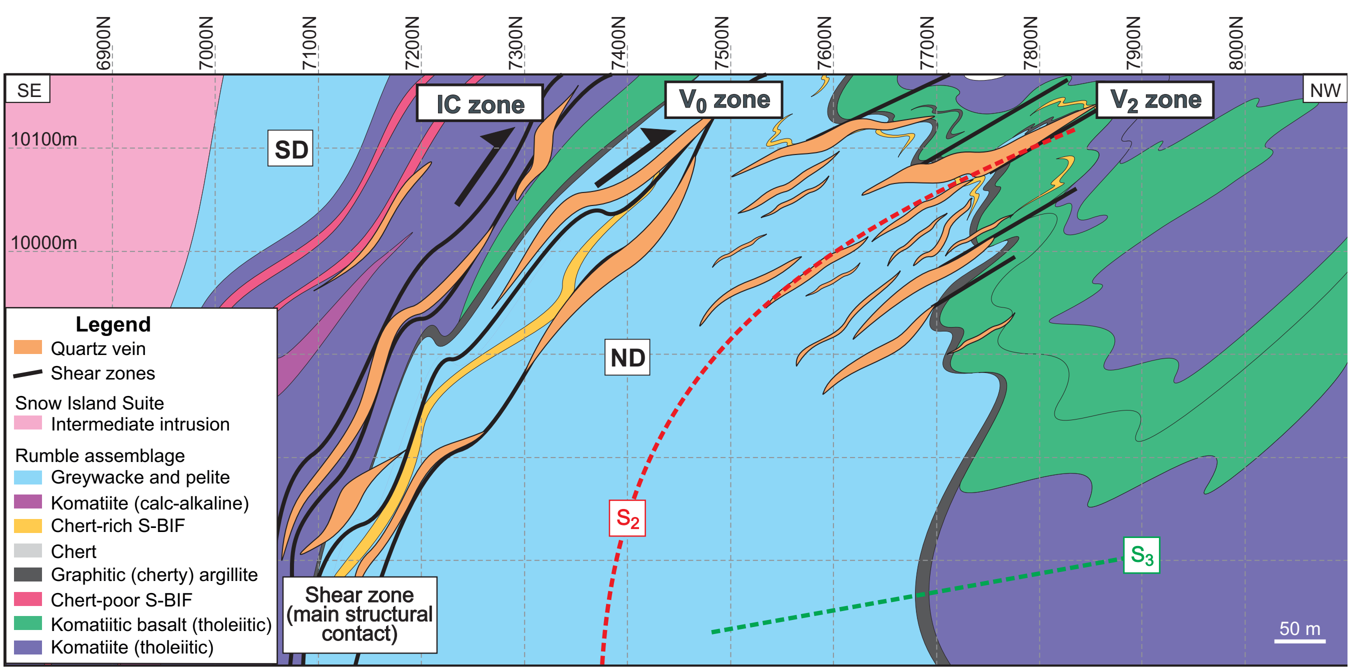

Figure 8. Interpretative cross-section of the IVR (15200 E) area based on drill section. *See* Figure 2 for the location of the section. Abbreviation: S-BIF = silicate-facies banded iron formation, SD = south domain.

alized envelope can extend for 800 m along strike, to 500 m below surface, and locally down to 730 m (Fig. 2, 7; Côté-Mantha et al., 2017). The southern and northern boundaries of the CD correspond to faults that delineate the contacts of the QZ and WT zones, respectively. To the south, the SD does not include any BIF nor gold zones. To the north and in the IVR area (Fig. 2), the contact between the komatiite and greywacke of the ND corresponds to the IC zones. The IC zones mainly consist of visible gold-bearing and sulphide-poor, shear-hosted and extensional quartz±calcite veins, which were folded, boudinaged, and recrystallized during D_2 deformation (Fig. 6c). These veins form an anastomosing network that is subparallel to the contact, which is now transposed parallel to S_2 schistosity. The komatiite is hydrothermally altered to a distal talcose and a proximal calcite-Mg-biotite-ripidolite-gersdorffite zone (Fig. 9d).

IVR Area

In the IVR area, the orebodies are mainly characterized by shallow to moderately (20–45°) southeast-dipping, auriferous quartz±calcite veins developed in high-strain corridors mostly affecting the tholeiitic mafic-ultramafic volcanic and sedimentary rocks (V zones; Fig. 8). These zones are transposed parallel to the S_2 schistosity and form a discontinuous anastomosing network of 3 to 15 m thick vein-rich corridors that extend for over 2000 m along strike, and down to at least 650 m depth (Fig. 8; Côté-Mantha et al., 2017). The alteration halo in the greywacke is characterized by proximal quartz-muscovite-calcite±apatite-tourmaline (Fig. 9g) and distal biotite-ripidolite assemblages. In the mafic volcaniclastic rocks, the distal and proximal assemblages are composed of ripidolite-clinozoisite-titanite and calcite-actinolite, respectively. The gold distribution in the V zones is usually less continuous and more erratic than the replacement-style orebodies, due to a strong nugget effect. The V zones typically yield intervals of 8 to 10 g/t Au over 4 to 5 m intervals (Côté-Mantha et al., 2017).

DISCUSSION

The presence of different styles of mineralization at Amaruq is considered a result of contrasting rheology and geochemistry of the host sequence. The main mechanisms of gold precipitation are attributed to fluid/pressure fluctuations (structural traps), and to fluid/rock interactions (lithological and geochemical traps; cf. Mikucki, 1998). The S-BIFs at Whale Tail, and to some extent at IVR, are the principal hosts of the disseminated-style orebodies, acting as a redox trap. The other lithologies are less favourable hosts for disseminated Au mineralization because of their low Fe-content, such as ultramafic volcanic rocks. In this less favourable lithology, the presence of carbonate facilitates the acidification of reacting fluid that promotes localized and sporadic precipitation of native gold ±arsenopyrite, instead of dissemination within the altered rocks (Fig. 9d; cf. Mikucki, 1998).

The study of the Amaruq area shows that two volcanic sequences are present with distinct petrographic, geochemical, and metallogenic features. The tholeiitic mafic-ultramafic rocks of the ND have a komatiitic affinity and are interlayered with chert-poor S-BIF. A large part of the auriferous quartz±carbonate auriferous veins of the V and IC zones are hosted in the ND volcanic rocks (Fig. 3, 4, 7, 8). In contrast, transitional to calc-alkaline mafic-ultramafic rocks of the SD are enriched in light REEs, and devoid of S-BIF and auriferous zones (Fig. 3, 4, 7). The structural nature of the contact between the barren SD and the ore-hosting CD, and the complete absence of mineralized and altered rocks in the SD, strongly suggest that this structural contact represents a major discontinuity. At Meadowbank, the bulk of the gold mineralization is also localized along an inferred major tectonic contact between two structurally juxtaposed volcano-sedimentary successions of slightly different ages (i.e. ca. 2717 and 2711 Ma) that may have acted as a major structure and hydrothermal fluid pathway (Janvier et al., 2015; Janvier, 2016).

Figure 9 (opposite page). a) Replacement-style zone of “silica flooding” in chert-rich silicate-facies banded iron formation (S-BIF) associated with granoblastic arsenopyrite±löllingite and textural characteristics of gold from the QZ zones. **b)** Stratabound and discordant disseminated Ca-amphibole-pyrrhotite and siderophyllite-arsenopyrite±Fe-gersdorffite and gold characterizing the replacement-style ore in chert-poor S-BIF of the WT zones. **c)** Quartz-Ca-amphibole-calcite veins with an albite-epidote proximal alteration zone, which are part of the QZ zones hosted in the chert (sample with 0.9 g/t Au). **d)** Shear zones and quartz-calcite vein hosted in the komatiite with biotite-talc proximal alteration characteristic of the IC zone (sample with 1.7 g/t Au). **e)** Backscatter photomicrograph of the replacement-style zone of “silica flooding” in chert-rich S-BIF showing the retrograde textural relationship between gold, löllingite, and arsenopyrite (sample with 18.1 g/t Au). **f)** Reflected light photomicrograph of the replacement-style ore and associated sulphide minerals in chert-poor S-BIF (sample with 4.7 g/t Au). **g)** Reflected light photomicrograph of native free gold and pyrrhotite in quartz-rich gangue characteristic of the quartz vein-style mineralization (88.9 g/t Au). **h)** Photograph of auriferous quartz±muscovite-arsenopyrite-pyrrhotite veins hosted in greywacke. Abbreviations: Ab = albite, Act = actinolite, Apy = arsenopyrite, Au = gold, Bt = biotite, Cal = calcite, Chl = chlorite, Czo = clinozoisite, Gers = gersdorffite, Grt = garnet, Lö = löllingite, Ms = muscovite, Oli = oligoclase, Po = pyrrhotite, Qtz = quartz, Rp = ripidolite, Sid = siderophyllite, Stp = stilpnomelane, Tc = talc, Ts = tschermakite.

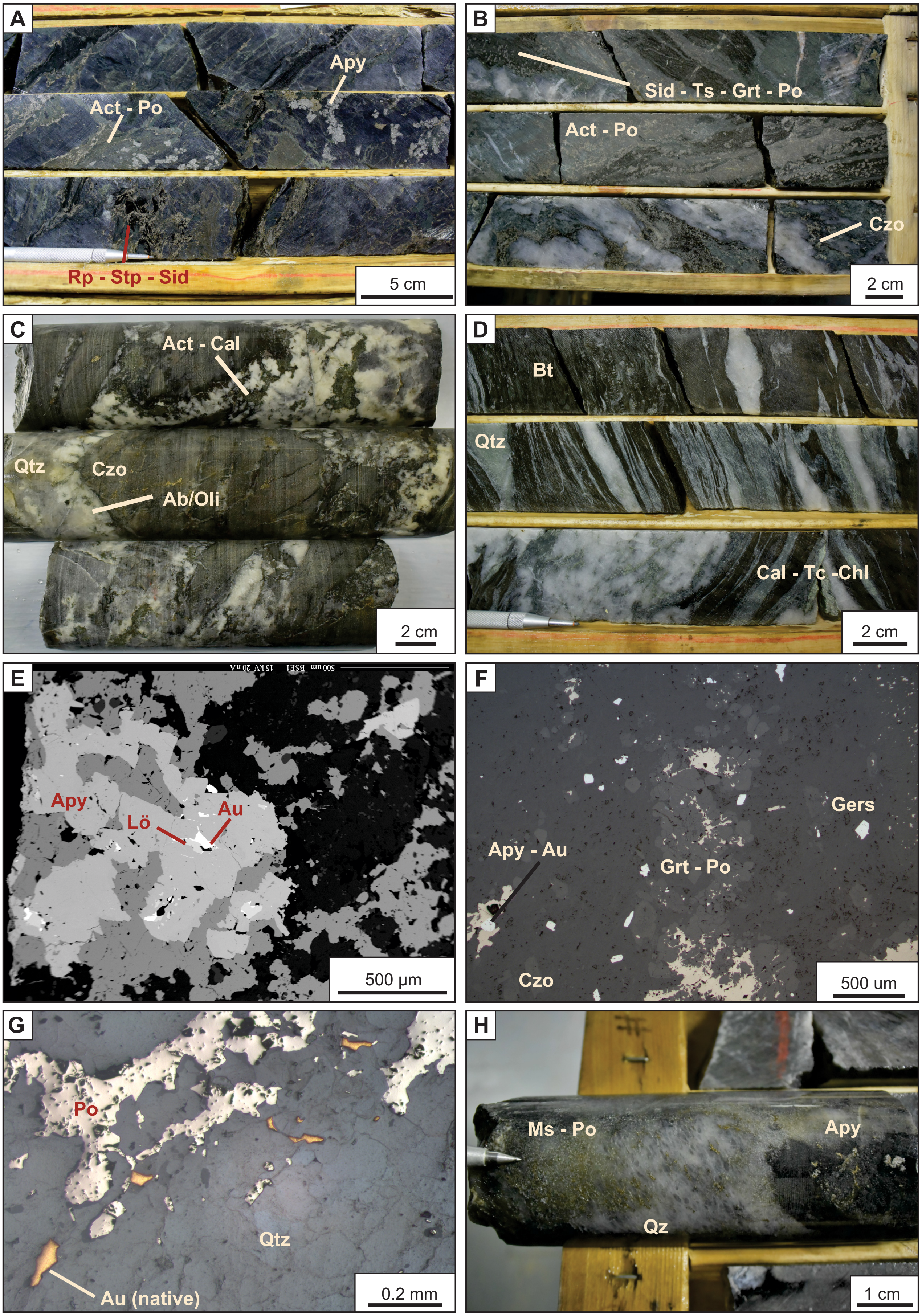
A
Apy
Act - Po
Rp - Stp - Sid
5 cm
B
Sid - Ts - Grt - Po
Act - Po
Czo
2 cm
C
Act - Cal
Qtz
Czo
Ab/Oli
2 cm
D
Bt
Qtz
Cal - Tc -Chl
2 cm
E
Apy
Lö
Au
500 µm
F
Gers
Apy - Au
Grt - Po
Czo
500 um
G
Po
Qtz
Au (native)
0.2 mm
H
Ms - Po
Apy
Qz
1 cm

Detailed studies of the Meadowbank, Amaruq, Meliadine, and Three Bluffs systems have documented the fundamental role of the Paleoproterozoic deformation in the localization of gold in the Woodburn Lake group and other greenstone belts of the western Churchill Province (Sanborn-Barrie et al., 2014; Janvier et al., 2015; Lawley et al., 2015, 2016; Janvier, 2016; Valette et al., 2018). Gold mineralization is associated with sulphidized BIF, and localized within hinge zones of F_2 folds and/or along D_1 (D_{P1}) and/or D_2 (D_{P2}) brittle-ductile shears zones, which were the key parameters in controlling the gold distribution (Sanborn-Barrie et al., 2014; Janvier et al., 2015; Lawley et al., 2015, 2016; Janvier, 2016; Valette et al., 2018). At Amaruq, the vein- and replacement-style orebodies are characterized by shallow (20°) east-plunging ore shoots subparallel to the colinear F_2 and F_3 fold axes, as well as L_{2-3} intersection lineation. In the CD, moderately to steeply (65°) southwest-dipping ore shoots are locally present, especially on the south-dipping limbs of the asymmetric F_3 folds, which correspond to the stretching lineation developed during F_2 folding.

Although there is a recognized orogen-scale Trans-Hudsonian gold event in the western Churchill Province (e.g. Lawley et al., 2020), ongoing geochronology and field observations at Amaruq suggest a possible pre-Trans-Hudsonian epigenetic gold mineralizing event. Gold, or part of it, may have been initially introduced earlier, either during the Neoarchean and/or Paleoproterozoic, as suggested for the Meliadine district (Lawley et al., 2015, 2016). The Amaruq area may have preserved elements of deformation and metamorphism (and hydrothermal activity?) of the Arrowsmith Orogeny, as suggested by preliminary Re-Os ages of arsenopyrite, which are systematically older than 2.3 Ga (Mercier-Langevin et al., 2018).

IMPLICATIONS FOR EXPLORATION

Orogenic gold deposits in Precambrian greenstone belts are commonly located in the vicinity of first-order, deep-reaching crustal-scale fault zones, which allow fluid migration and vein filling of lower order shear zones and faults (e.g. Sibson et al., 1988; Groves et al., 1998; Dubé et Gosselin, 2007). Even if such a major structure has not yet been identified with confidence in the Amaruq area, lithological contacts are the locus of fertile conduits that are parallel to the northeast regional structural grain. Ore-forming hydrothermal fluids were focused along these contacts during regional deformation and metamorphism. D_2 (or D_1) high-strain brittle-ductile deformation zones, F_2 fold limbs, and/or fold hinge zones are the main structural parameters that can be used as gold metallotects in the Woodburn Lake greenstone belt. Chemical sedimentary and/or high-Fe units along with Ca-metasomatism and potassic±sodic alterations are also key lithological and geochemical parameters to consider. Identification of such key geological parameters and a better documentation of the absolute and relative timing of gold events in areas of superimposed deformation and metamorphism, are crucial for effective mineral exploration and targeting of BIF-hosted orogenic gold deposit in the Churchill Province and other Archean terranes affected by Paleoproterozoic orogenesis.

FUTURE/ONGOING WORK

Geochemical characteristics of the Amaruq deposit hydrothermal footprint are currently being studied and preliminary data are not presented in this report for conciseness. Other analytical work is still underway: 1) thermobarometry of silicate and sulphide minerals will allow estimation of the pressure and temperature conditions of the main metamorphic event(s), as well as fluid temperature during retrograde metamorphism and gold exsolution; 2) silicate and sulphide mineral chemistry analyses by scanning electron microscope (SEM) and laser ablation-inductively coupled plasma mass spectrometry (LA-ICP-MS) to constrain the composition of the ores and ore-forming conditions; 3) U-Pb and $^{40}Ar/^{39}Ar$ geochronology studies of zircon/titanite and amphibole/muscovite, respectively, to date the mafic(-ultramafic) volcanic rocks and cooling of the hydrothermal system; and 4) Re-Os dating of arsenopyrite and LA-ICP-MS elementary maps are being refined to improve the understanding of the timing of gold mineralization at different scales. All the field observations and analytical data will be integrated to develop a model for the formation of the BIF-hosted Amaruq gold deposit and to contribute to improved exploration models.

ACKNOWLEDGMENTS

This report is a contribution to NRCan's Targeted Geoscience Initiative Program (TGI-5). Support for this study was provided through the Gold Project and activity G-2.4: Lithologic and tectonic controls on Paleoproterozoic BIF-hosted/associated gold. This work is part of an ongoing MITACS supported Ph.D. study by M. Valette at the Université du Québec à Montréal (UQÀM). We thank Agnico Eagle Mines Ltd. for access to their property, drill core and databases, and for scientific, logistical, and financial support throughout the project. This report benefited from the reviews of Z. Toth and S. Castonguay. We also acknowledge E. Ambrose and V. Bécu for their editorial handling and technical reviews.

REFERENCES

Annesley, I.R., 1990. Petrochemistry of the Woodburn Lake group komatiitic suite, Amer Lake, N.W.T., Canada; Ph.D. thesis, University of Ottawa, Ottawa, Ontario, 523 p.

Armitage, A.E., 1996. Geology and petrology of gold-bearing banded iron formation Keewatin district, Northwest Territories; M.Sc. thesis, Laurentian University, Sudbury, Ontario, 161 p.

Berman, R.G., 2010. Metamorphic map of the western Churchill Province, Canada; Geological Survey of Canada, Open File 5279, 49 p., 3 sheets, scale 1:2 500 000.

Berman, R.G., Ryan, J.J., Tella, S., Sanborn-Barrie, M., Stern, R., Aspler, L., Hanmer, S., and Davis, W., 2000. The case of multiple metamorphic events in the Western Churchill Province: evidence from linked thermobarometric and in-situ SHRIMP data, and jury deliberations; GeoCanada 2000 Conference, Extended Abstracts, CD-ROM, Abstract 836.

Berman, R.G., Sanborn-Barrie, M., Stern, R.A., and Carson, C.J., 2005. Tectonometamorphism at ca. 2.35 and 1.85 Ga in the Rae domain, western Churchill Province, Nunavut, Canada: insights from structural, metamorphic and in situ geochronological analysis of the southwestern Committee Bay belt; The Canadian Mineralogist, v. 43, p. 409–442.

Berman, R.G., Davis, W.J., and Pehrsson, S., 2007. Collisional Snowbird tectonic zone resurrected: Growth of Laurentia during the 1.9 Ga accretionary phase of the Hudsonian orogeny; Geology, v. 35, p. 911–914.

Berman, R.G., Pehrsson, S., Davis, W.J., Ryan, J.J., Qui, H., and Ashton, K.E., 2013. The Arrowsmith orogeny: Geochronology and thermobarometric constraints on its extent and tectonic setting in the Rae craton, with implications for pre-Nuna supercontinent reconstruction; Precambrian Research, v. 232, p. 44–69.

Boström, K., 1973. The origin and fate of ferromanganoan active ridge sediments; Stockholm; Contributions in Geology, v. 27, p. 147–243.

Calhoun, L., 2017. Lithostratigraphy and structure of the eastern Amer Group, Nunavut: Using combined surface mapping and enhanced sub-surface geophysical data; M.Sc. thesis, University of New Brunswick, Fredericton, New Brunswick, 166 p.

Côté-Mantha, O., Gosselin, G., Vaillancourt, D., and Blackburn, A., 2017. The Amaruq deposit – Building a customized toolset and using a flexible geomodel: Optimization from discovery to mine development; *in* Proceedings of Exploration 17, (ed.) V. Tschirhart and M.D. Thomas; Sixth Decennial International Conference on Mineral Exploration, 2017, p. 553–567.

Davies, T., Richards, J.P., Creaser, R.A., Heaman, L.M., Chacko, T., Simonetti, A., Williamson, J., and McDonald, D.W., 2010. Paleoproterozoic age relationships in the Three Bluffs Archean iron formation-hosted gold deposit, Committee Bay greenstone belt, Nunavut, Canada; Exploration and Mining Geology Journal, v. 19, p. 55–80.

Dubé, B. and Gosselin, P., 2007. Greenstone-hosted quartz-carbonate vein deposits; *in* Mineral Deposits of Canada: A synthesis of Major Deposit-Types, District Metallogeny, the Evolution of Geological Provinces, and Exploration Methods, (ed.) W.D. Goodfellow; Geological Association of Canada, Mineral Deposits Division, Special Publication, No. 5, p. 49–73.

Groves, D.I., Goldfarb, R.J., Gebre-Mariam, M., Hagemann, S.G., and Robert, F., 1998. Orogenic gold deposits: A proposed classification in the context of their crustal distribution and relationship to other gold deposit types; Ore Geology Reviews, v. 13, p. 7–27.

Janvier, V., Castonguay, S., Mercier-Langevin, P., Dubé, B., Malo, M., McNicoll, V.J., Creaser, R.A., de Chavigny, B., and Pehrsson, S.J., 2015. Geology of the banded iron formation-hosted Meadowbank gold deposit, Churchill Province, Nunavut; *in* Targeted Geoscience Initiative 4: Contributions to the understanding of Precambrian lode gold deposits and implications for exploration, (ed.) B. Dubé and P. Mercier-Langevin; Geological Survey of Canada, Open File 7852, p. 255–269.

Janvier, V., 2016. Géologie du gisement d'or Meadowbank encaissé dans des formations de fer rubanées, Nunavut, Canada; Ph.D. thesis, Institut national de la recherche scientifique – Centre Eau Terre Environnement, Québec, Quebec, 472 p.

Jefferson, C.W., White, J.C., Young, G.M., Patterson, J., Tschirhart, V.L., Pehrsson, S.J., Calhoun, L., Rainbird, R.H., Peterson, T.D., Davis, W.J., Tella, S., Chorlton, L.B., Scott, J.M.J., Percival, J.A., Morris, W.A., Keating, P., Anand, A., Shelat, Y., and MacIsaac, D., 2015. Outcrop and remote predictive geology of the Amer Belt and basement beside and beneath the northeast Thelon Basin, in parts of NTS 66-A, B, C, F, G and H, Kivalliq Region, Nunavut; Geological Survey of Canada, Open File 7242, 1 sheet.

Jensen, L.S., 1976. A new cation plot for classifying subalkalic volcanic rocks; Ontario Ministry of Natural Resources, Miscellaneous Paper 66, 22 p.

Kerswill, J.A., Goff, S.P., Wilkinson, L., Jenner, G.A., Kjarsgaard, B.A., Bretzlaff, R., and Samaras, C., 1998. An update on the metallogeny of the Woodburn Lake group, western Churchill province, Northwest Territories; *in* Current Research 1998-C; Geological Survey of Canada, p. 29–41.

Lauzon, M.-C., Mercier-Langevin, P., Valette, M., Beaudoin, G., De Souza, S., Côté-Mantha, O., and Simard, M., 2020. Ore mineralogy and mineral chemistry of the Whale Tail zone, Amaruq gold deposit, Nunavut; *in* Targeted Geoscience Initiative 5: Contributions to the Understanding of Canadian Gold Systems, (ed.) P. Mercier-Langevin, C.J.M. Lawley, and S. Castonguay; Geological Survey of Canada, Open File 8712, p. 267–279. doi:10.4095/326044

Lawley, C.J.M., Creaser, R.A., Jackson, S.E., Yang, Z., Davis, B.J., Pehrsson, S.J., Dubé, B., Mercier-Langevin, P., and Vaillancourt, D., 2015. Unraveling the Western Churchill Province Paleoproterozoic gold metallotect: Constraints from Re-Os arsenopyrite and U-Pb xenotime geochronology and LA-ICP-MS arsenopyrite trace element chemistry at the BIF-hosted Meliadine gold district, Nunavut, Canada; Economic Geology, v. 110, p. 1425–1454.

Lawley, C.J.M., McNicoll, V., Sandeman, H., Pehrsson, S., Simard, M., Castonguay, S., Mercier- Langevin, P., and Dubé, B., 2016. Age and geological setting of the Rankin Inlet greenstone belt and its relationship to the gold endowment of the Meliadine gold district, Nunavut, Canada; Precambrian Research, v. 275, p. 471–795.

Lawley, C.J.M., Selby, D., Davis, W.J., Yang, E., Zhang, S., Jackson, S.E., Petts, D.C., O'Connor, A.R., and Schneider, D.A., 2020. Paleoproterozoic gold and its tectonic triggers and traps: Implications from Re-Os sulphide and U-Pb detrital zircon geochronology, Lynn Lake, Manitoba; *in* Targeted Geoscience Initiative 5: Contributions to the Understanding of Canadian Gold Systems, (ed.) P. Mercier-Langevin, C.J.M. Lawley, and S. Castonguay; Geological Survey of Canada, Open File 8712, p. 211–222. doi:10.4095/326033

MacLean, T.J. and Barrett W.H., 1993. Lithogeochemical techniques using immobile elements; Journal of Geochemical Exploration, v. 48, p. 109–133.

McDonough, W.F. and Sun, S.S., 1995. The composition of the Earth; Chemical Geology, v. 120, p. 223–253.

McNicoll, V., Thériault, R.J., and McDonough, M.R., 2000. Taltson basement gneissic rocks: U-Pb and ND isotopic constraints on the basement to the Paleoproterozoic Taltson magmatic zone, northeastern Alberta; Canadian Journal of Earth Sciences, v. 38, p. 1575–1596.

Mercier-Langevin, P., Valette, M., De Souza, S., Creaser, R.A., McNicoll, V., Grondin-Leblanc, P., St-Pierre, B., Lauzon, M.-

C., Malo, M., Côté-Mantha, O., and Simard, M., 2018. Lithologic controls on Paleoproterozoic BIF-hosted/associated gold: Overview of Re-Os geochronology and Pb isotopes preliminary results; *in* Targeted Geoscience Initiative: 2017 report of activities, volume 1, (ed.) N. Rogers; Geological Survey of Canada, Open File 8358, p. 147–152.

Mikucki, E.J., 1998. Hydrothermal transport and depositional processes in Archean lode-gold systems: A review; Ore Geology Reviews, v. 13, p. 307–321.

Pehrsson, S.J., Wilkinson, L., Zaleski, E., Kerswill, J., and Alexander, B., 2000. Structural geometry of the Meadowbank deposit area, Woodburn Lake Group – Implications for genesis of a major gold deposit in the Western Churchill Province; A Contribution to the Western Churchill NATMAP Project, Geological Survey of Canada, 4 p.

Pehrsson, S.J., Berman, R.G., and Davis, W.J., 2013a. Paleoproterozoic orogenesis during Nuna aggregation: A case study of reworking of the Rae craton, Woodburn Lake, Nunavut; Precambrian Research, v. 232, p. 167–188.

Pehrsson, S.J., Berman, R.G., Eglington, B., and Rainbird, R., 2013b. Two Neoarchean supercontinents revisited: The case for a Rae family of cratons; Precambrian Research, v. 232, p. 27–43.

Sanborn-Barrie, M., Davis, W.J., Berman, R.G., Rayner, N., Skulski, T., and Sandman, H., 2014. Neoarchean continental crust formation and Paleoproterozoic deformation of the central Rae craton, Committee Bay belt, Nunavut; Canadian Journal of Earth Sciences, v. 51, p. 635–667.

Sherlock, R., Pehrsson, S.J., Logan, A.V., Hrabi, R.B., and Davis, W.J., 2004. Geological setting of the Meadowbank gold deposits, Woodburn Lake group, Nunavut; Exploration and Mining Geology, v. 13, p. 67–107.

Sibson, R.H., Robert, F., and Poulsen, K.H., 1988. High-angle reverse faults, fluid-pressure cycling, and mesothermal gold-quartz deposits; Geology, v. 16, p. 551–555.

Spry, P.G., Peter, J.M., and Slack, J.F., 1998. Meta-exhalites as exploration guides to ore; *in* Metamorphosed and Metamorphogenic Ore Deposits, (ed.) P.G. Spry, B. Marshall, and F.M. Vokes; Reviews in Economic Geology, v. 11, p. 167–204.

Valette, M., De Souza, S., Mercier-Langevin, P., McNicoll, V.J., Grondin-LeBlanc, P., Côté-Mantha, O., Simard, M., and Malo, M., 2018. Lithological, hydrothermal, structural and metamorphic controls on the style, geometry and distribution of the auriferous zones at Amaruq, Churchill Province, Nunavut; *in* Targeted Geoscience Initiative: 2017 report of activities, volume 1, (ed.) N. Rogers; Geological Survey of Canada, Open File 8358, p. 153–156.

Zaleski, E., 2005. Geology, Meadowbank River area, Nunavut; Geological Survey of Canada, Map 2068A, scale 1:50 000.